RESEARCH PAPER

On the effects of austenite phase transformation on welding residual stresses in non-load carrying longitudinal welds

Jonas Hensel · Thomas Nitschke-Pagel · Klaus Dilger

Abstract Residual stresses affect the fatigue strength of welded structures and components. A common sample type used for studies on residual stress effects is the fillet-welded longitudinal gusset. This sample type shows in fatigue tests significant residual stress effects. But the mechanisms of residual stress generation are not clarified for this sample type yet. High tensile residual stresses in the surface layer near the weld toe could not be proven by experimental methods but are generally assumed. Here presented are results from experimental and numerical investigations on welding residual stress generation. Specimens with single and multilayer fillet welds have been produced as well as simplified curved multilayer deposition welds studying residual stress build-up. Temperature measurements have been conducted during welding examining the influence of austenite phase transformation. Residual stresses have been determined by means of X-ray diffraction at the surface as well as by neutron diffraction over specimen thickness. Further, the mechanisms of residual stress build-up have been evaluated by finite element calculations. It could be shown that the austenite phase transformation has significant effect on the residual stresses near the weld toe also for this sample type.

Keywords Residual stresses · Longitudinal welds · X-rays · Neutron radiation · Diffraction · Austenite

J. Hensel (✉) · T. Nitschke-Pagel · K. Dilger
Institute of Joining and Welding, Technische Universität
Braunschweig, Langer Kamp 8, Braunschweig, Germany
e-mail: j.hensel@tu-braunschweig.de

1 Introduction

Welding is common in all engineering fields and is often used for steel structures that are loaded by vibration loading. The fatigue strength of welded structures and components is influenced by many parameters which characterize the loading itself or the weld. Among the parameters affecting the fatigue strength are welding-induced residual stresses. Tensile residual stresses are suspected to decrease the allowed stresses in welded components whereas compressive residual stresses increase allowable stresses. The effectiveness of residual stresses also depends on the local material characteristics, such as hardness and yield strength. For steel base metal, this is known as the susceptibility of the material to residual stresses [1, 2] and can also be transferred to welded joints [3]. Apart from allowable stress levels, the knee point position of design S-N curves is also suspected to be affected by residual stresses. For instance, [4] observed a shift of the knee point position for steel plates with fillet-welded longitudinal stiffeners to a lower number of load cycles by thermal stress relief. This was explained by relieving high tensile residual stresses. Furthermore, residual stresses affect the brittle fracture behavior, the crack propagation rate and they must always be considered in combination with welding distortion.

For the evaluation of the influence of residual stresses on fatigue strength, it is common to compare fatigue test results from small-scale specimens in as-welded condition and from thermally stress-relieved specimens. Thermal stress relief of welded components is also common in engineering practice to ensure that tensile residual stresses from welding or machining are removed. Even though course residual stress states were documented before and after thermal treatment in many research reports, this is not always done for the location of fatigue crack initiation. Of course, thermal treatment may be less functional or even ineffective in cases where residual stresses in the as-welded state are lower than expected. This

can be problematic, especially since even design rules, e.g., [5] allow beneficial treatment of stress-relieved components without the requirement that residual stress relief is proven. Further, wrong conclusions might be drawn from S-N data if residual stress effects are observed without precise knowledge about residual stress distribution at the location of crack growth. This is a specific issue of fatigue strength data basis used for design guidelines and the motivation of this work.

Residual stresses in steel plates with fillet-welded longitudinal gussets were determined in several investigations before. But residual stresses were not always determined at the location of crack initiation (weld toe), for instance due to geometrical constraints like overlapping weld metal [6]. In many investigations, such as [6–9], residual stresses were determined at a distance of 1 or 2 mm apart the weld toe. The magnitude of residual stresses in the weld toe was derived from extrapolations based on these investigations. Thus high tensile residual stresses were assumed generally and used for the explanation of results from fatigue testing. In other investigations [10–12] and own publications [13, 14], residual stresses were also determined directly at the weld toe. It was found there that residual stresses in general did not reach the yield strength of the base metal at the weld toe and were considerably lower than the highest magnitudes found some millimeters apart the weld toe. This could be observed for steels with yield strengths between 300 and 1,000 MPa. Some interesting findings could also be made by relating the reported magnitude of the residual stresses from literature data to the reported yield strength and plotting the ratios over the actual location of measurement. Figure 1 shows the ratios of residual stresses and yield strengths of the base metal for steels with yield strengths f_y between 300 and 460 MPa as well as between 670 and 1000 MPa. An increasing trend can be seen for the first group. Residual stresses directly at the weld toe approximately reached 5 to 25 % of the yield strength,

whereas 60 to 80 % of the yield strengths were reached at a distance of 1 mm. Relatively low residual stresses in comparison to the yield strength were found in the case of the high-strength steel. The ratio of residual stresses to the yield strength at the weld toe was between −5 % (compression) and 30 %. However, although the literature on the magnitudes and distributions of residual stresses is in good agreement this data does not match the reported effects on fatigue strength reduction. In the following the mechanisms of residual stress generation near the weld toe will be clarified.

2 General remarks

Residual stresses discussed here are considered in macroscopic scale [15]. That means that residual stresses are in equilibrium and are distributed over several grains. Further, it is necessary to define a terminology for the directions of residual stresses in relation to the weld. In general, residual stresses in loading direction are of interest. The terminology used by the authors always refers to the direction of welding as common for butt welds. Residual stresses in welding direction are termed "longitudinal residual stresses" and residual stresses perpendicular to the welding direction are termed "transverse residual stresses". The point of interest of the specimen type discussed here is always the origin of crack initiation at the face sides of the stiffeners. The residual stresses in loading direction are oriented perpendicular to the weld at this point and are transverse residual stresses, see Fig. 2. Residual stresses perpendicular to the loading direction are oriented in welding direction and are accordingly longitudinal residual stresses.

3 Residual stress generation in welded components

Residual stress generation in welds is a consequence of hindered shrinkage of heterogeneously heated material volumes. The weld and the heat-affected zone (HAZ) are surrounded by cooler zones that cause geometric constraints during cooling. For straight welds, these constraints in direction of welding are mainly controlled by the colder base metal beside the
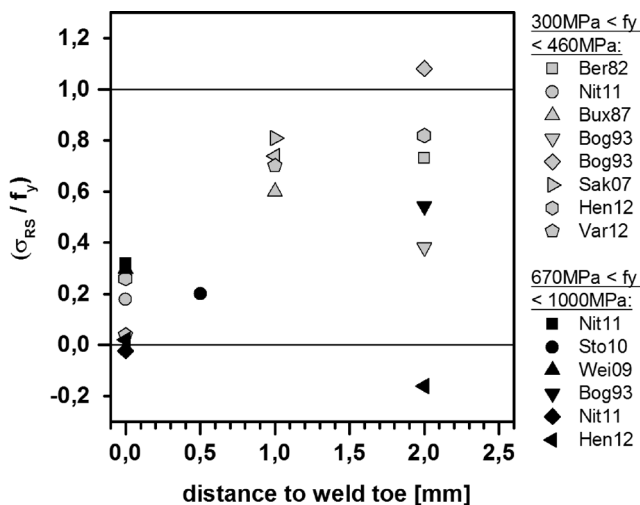
Fig. 1 Ratios of residual stresses to yield strength (σ_{RS}/f_y) at the weld toes of steel plates with longitudinal fillet-welded gussets
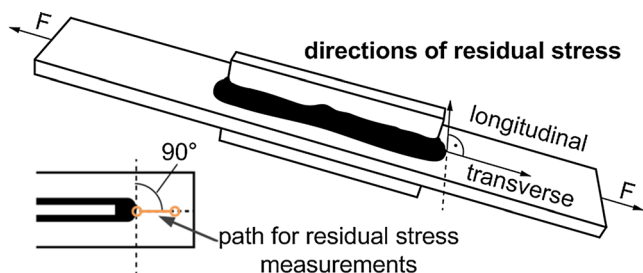
Fig. 2 Definition of the used terminology of residual stress directions at the welds of longitudinal stiffeners

weld. Perpendicular to the weld, the constraint depends strongly on the boundary conditions of the entire weld detail and the weld composition. If the weld detail is located within a large structure with high global stiffness, the constraint is consequently high. In the case of free edges, the composition of the weld becomes more critical. For single-layer welds, the constraint perpendicular to the weld is very low. In the case of multilayer welds, the constraints depend on the varying temperature profile over thickness. The constraint increases with increasing temperature gradient over the entire weld thickness. In general, tensile residual stresses are caused by these geometric constraints in the cooling zones and the height of the residual stresses depends on the order of the geometric constraints. For example, small-scale single-layer butt weld specimens that are welded without edge constraints are suspected to show low residual stresses perpendicular to the weld [16].

Another very important cause of residual stress generation in transforming steels is the hindered volume expansion during the austenite phase transformation [17]. This effect becomes more effective with increasing strength of the steel. Resulting residual stresses in transforming steels cannot be explained as straightforward as if only hindered shrinkage during cooling is effective. They are always a result of a combination of these two effects. Thus, it cannot be generally predicted how residual stresses develop, the height and distribution is strongly dependent on the temperature profiles, cooling rates, and of course the material characteristics.

The interaction of hindered shrinkage and hindered volume expansion can be demonstrated by the stress–temperature diagram according to [17], Fig. 3. Residual stresses are generated, due to the hindered shrinkage, with decreasing temperature. The magnitude of the residual stresses is limited by the increasing yield strength of the austenite. If the phase transformation occurs at high temperatures (generation of ferrite–pearlite phase) due to slow cooling rates, the compressive residual stresses from the phase transformation are limited to the low yield strength at elevated temperatures (curve 1). After completion of the phase transformation, the cooling goes on, and high tensile stresses from ongoing hindered shrinkage govern the resulting residual stress state. High cooling rates lead to a phase transformation at much lower temperatures (generation of bainite or martensite phase) resulting in generation of higher compressive residual stresses from hindered volume expansion (curves 2 and 3). Hindered shrinkage during further cooling leads to tensile residual stresses that are superposed with the compressive residual stresses from hindered volume expansion. The resulting magnitude of the residual stresses after cooling is therefore strongly dependent on the yield strength at the phase transformation temperature and the remaining temperature gradient at the end of the phase transformation. If the cooling rate is high, and thus the phase transformation occurs at low temperatures, low tensile or even compressive residual stresses can be expected.
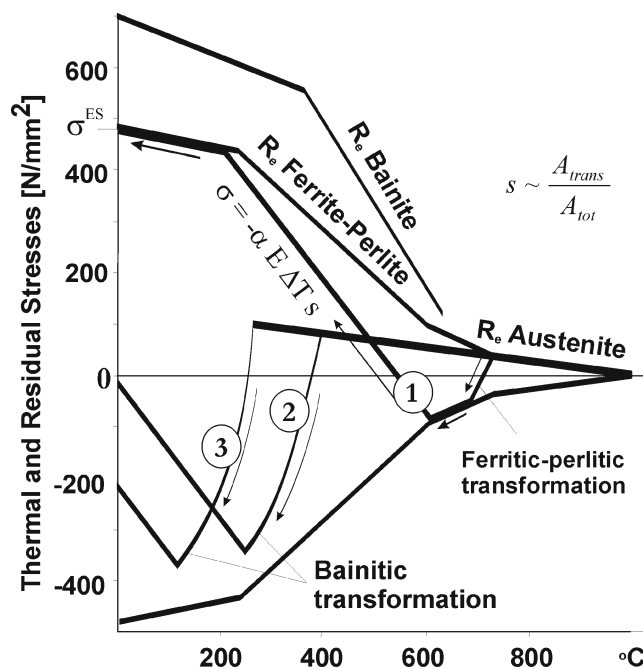

Fig. 3 Meaning of the interaction of hindered shrinkage and austenite phase transformation for residual stress generation in transforming steels [17]

Accordingly, the cooling rate has influence not only on the microstructure but also on the residual stresses. The schematic time-temperature-transformation diagram after [18], shown in Fig. 4, describes the correlation between heat input and residual stress generation. High tensile residual stresses are generated due to high-heat input in combination with relatively low hardness. Even higher heat input does not lead to a further increase of the transformation temperature. Instead, further increase of the heat input leads to decreasing tensile residual stresses. This can be explained by the decreasing constraint due to the elevated temperature of the entire specimen. The temperature gradients within the welded joint become automatically less with increasing heat input. But low-heat input leads to faster cooling rates and martensite phase. Hindered volume expansion becomes highly effective at low transformation temperature due to distinctive yield strength at martensite start temperature. In consequence, low tensile or even compressive residual stresses are generated in combination with a relatively high hardness. However, it must still be considered that the final residual stresses are always a result of the combined effects of hindered shrinkage and phase transformation. High global constraints of shrinking after welding can always lead to high tensile residual stresses.

4 Experimental work

The general mechanisms of residual stress generation in transforming steels described above can be used to explain

Fig. 4 Schematic time-temperature-transformation diagram for construction steels showing the interaction of heat input and residual stress generation [18]
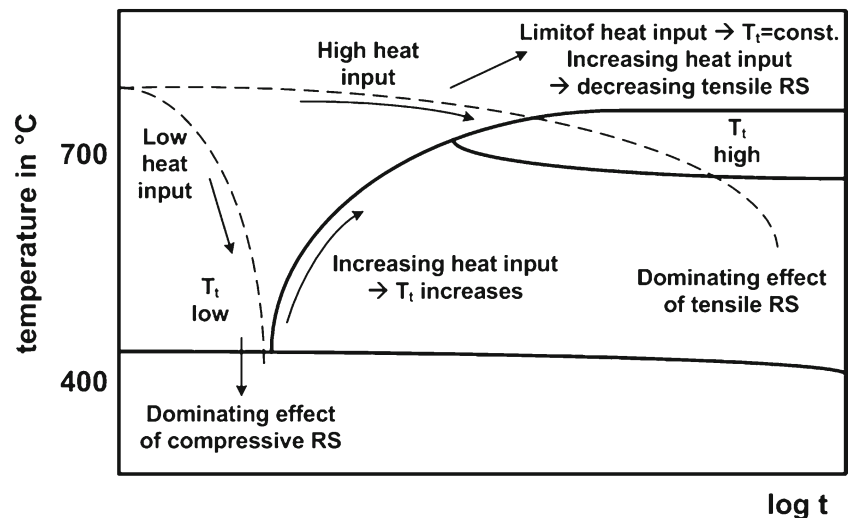
the residual stress build-up in arbitrary weld geometries. The following describes experimental work for the explanation of the residual stress generation around longitudinal fillet-welded gussets.

Welding experiments were conducted using three different setups. In a first setup deposition welds were welded on flat plates (thickness t=12 mm) without the stiffener. The weld geometry used was the same as for longitudinal stiffeners. Further specimens with attached longitudinal stiffeners were welded by either single-layer fillet welds (setup 2, t=10 mm) or by multilayer full depth fillet welds (setup 3, t=12 mm).

Residual stress measurements were done by means of X-ray diffraction using CrK_α radiation. The {211}-pattern was measured using 11 Ψ-angles. Residual stresses were calculated with the $\sin^2\Psi$-method with X-ray elastic constants of ½ s_2=6.08 mm²/N (ferrite).

4.1 Setup 1: residual stress build-up in curved deposit welds

In the first step, the geometry was simplified to single- and multilayer deposition welds, similar in shape to the real weld of longitudinal stiffeners. The deposition welds were welded on base plates without stiffener. The welding was performed by a robot-mounted GMA welding torch using EN ISO 14341-A-G4Si1 filler metal (1.2 mm). The plates were held down during welding by means of fasteners. The base plates had a thickness of 12 mm and were made from S355NL (f_y= 390 MPa) with the dimensions of 290 x 90 mm². The preheating and inter pass idle temperature for multilayer deposition welds was 20 °C.

For the first experiment, a multilayer weld was built up with the same welding parameters and the same weld geometry used for the specimen type "steel plate with fillet-welded longitudinal gusset" described in Section 4.2 in detail. The welding parameters for all layers were the same. Residual

stresses were determined by means of X-ray diffraction after each of the three layers in transverse direction at the short curved section of the weld, as shown in Fig. 5. It can be seen that transverse residual stresses after welding of the first layer showed a maximum of almost 300 MPa at a distance of 1 mm to the weld toe. In the direction to the weld toe, the residual stresses dropped slightly to 180 MPa at the weld toe. After welding of the second layer, the tension maximum was shifted further apart from the weld toe. The highest residual stresses could then be found 5 mm from the weld toe with a magnitude of 350 MPa. The welding of the third layer did not lead to a further change of the maximum residual stresses, but the residual stresses in the HAZ decreased further to 20 MPa.

In the second experiment, only the first of the three layers was welded, but the preheating temperature was varied. The first specimen was welded at room temperature (20 °C), the second specimen was preheated to 100 °C and the third to 200 °C. This was done to increase the heat input and to decrease the cooling rate. The cooling times from 800 to 500 °C ($t_{8/5}$) were determined at the short sides of the deposition welds by means of K-type thermocouples (diameter 0.5 mm) and are shown in Table 1. It can be seen that the cooling time increased from 2.4 s (20 °C) to 8.8 s (200 °C) with increasing preheating temperature.

Resulting residual stresses are shown in Fig. 6. Whereas the residual stresses from the single-layer deposit weld at room temperature showed the same profile as for the first layer shown in Fig. 5, preheating led to a change of the residual stress profiles. Preheating to 100 °C reduced the highest residual stresses slightly to 200 MPa. But in this case, the maximum could be found directly at the weld toe. With increasing distance to the weld toe, the residual stresses dropped continuously. A further increase of the preheating temperature to 200 °C led to a further decrease of the tensile residual stresses. Directly at the weld toe residual stresses

Fig. 5 Deposition welding on S355NL. Residual stresses build-up in a multilayer weld
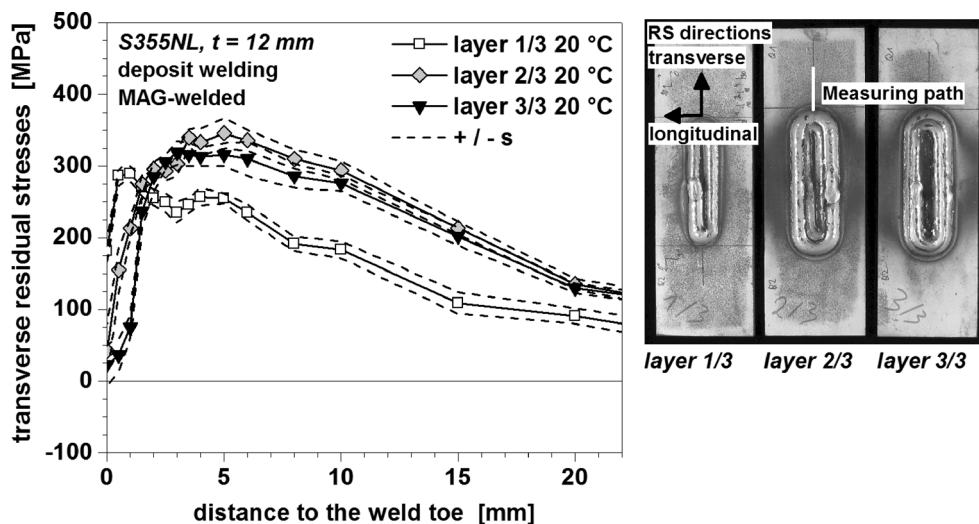
became close to zero, whereas small tensile residual stresses of 80 MPa were still present in a distance of 6 to 7 mm from the weld toe.

4.2 Setup 2: longitudinal stiffeners with single-layer fillet welds

For the second experimental setup, longitudinal stiffeners were attached to base plates with single-layer fillet welds. The specimens were made of different steel grades, S355N ($f_{y,min}$=360 MPa), S690Q ($f_{y,min}$=690 MPa) and S960Q ($f_{y,min}$=960 MPa) [13]. The base plate of the specimens had dimensions of 300 x 75 mm^2 and a thickness of 10 mm. Longitudinal gussets were attached at both sides symmetrically with dimensions of 75 x 35 mm^2 and a thickness of 10 mm. The specimens were prepared using a robot-mounted GMA welding torch without preheating. The temperature at weld begin was equal to the ambient temperature (20 °C). The welding wire had a diameter of 1.2 mm (S355N/EN ISO 14341-A: G3Si1, S690Q/EN ISO 16834-A: G69 6M21 Mn3Ni2.5CrMo and S960Q/EN ISO 16834-A: G 89 6M Mn4Ni2CrMo). The samples were held down during welding by fasteners. The welding was started and stopped at the same location in the middle of the sample at half length of the stiffeners. At the short

sides of the stiffeners, the torch was 180° turned. The welding voltage was 28 V, the current 220 A at varying welding velocity controlling the heat input. At the long sides of the stiffeners, welding velocity was at 30 cm/min and at the short sides 65 cm/min. This high welding velocity was necessary to avoid undercuts due to the turn of the welding torch at small radius.

Residual stress measurements were conducted on two samples of each material along all four weld toes. Figure 7 presents the determined residual stresses from all four sections as well as the average of all measurements. Shown are residual stresses in load direction (perpendicular to the weld). The highest residual stresses in samples made from S355N exceeded the nominal yield strength of the base metal. The maximal magnitude was 520 MPa at a distance of approximately 2 mm from the weld toe. Higher strength steels (S690Q and S960Q) showed lower residual stresses with magnitudes of approximately 40 % of the nominal yield strength. Residual stresses at the weld toe were smaller than the maxima determined and varied between -80 MPa (compression) and 200 MPa (tension).

Compressive residual stresses were observed for S355N and S690Q in the base metal. This resulted from clean blasting before welding to remove the mill scale. Samples made of S960Q were also clean blasted but thermally stress relieved afterwards.

4.3 Setup 3: multilayer fillet welds

The third setup used for experimental investigations was for GMA welding of multilayer welds. Longitudinal attachments were attached at both sides of the base plate by three layers each. The weld was performed as full-penetration joint using S355NL and S960QL. The dimensions of the base plate and the attached gussets were 400 x 60 x 12 mm^3 and 150 x 30 x 12 mm^3, respectively. The parameters used for

Table 1 Cooling times in dependence of the preheating temperature for curved single-layer deposit welds determined at the short side of the weld

| Preheating temperature	Determined cooling-times $t_{8/5}$ (800 to 500 °C)
Room temperature (20 °C)	2.4 s
100 °C	4.4 s
200 °C	8.8 s

Fig. 6 Deposition welding on S355NL. Influence of cooling rate on residual stress generation at the weld toe
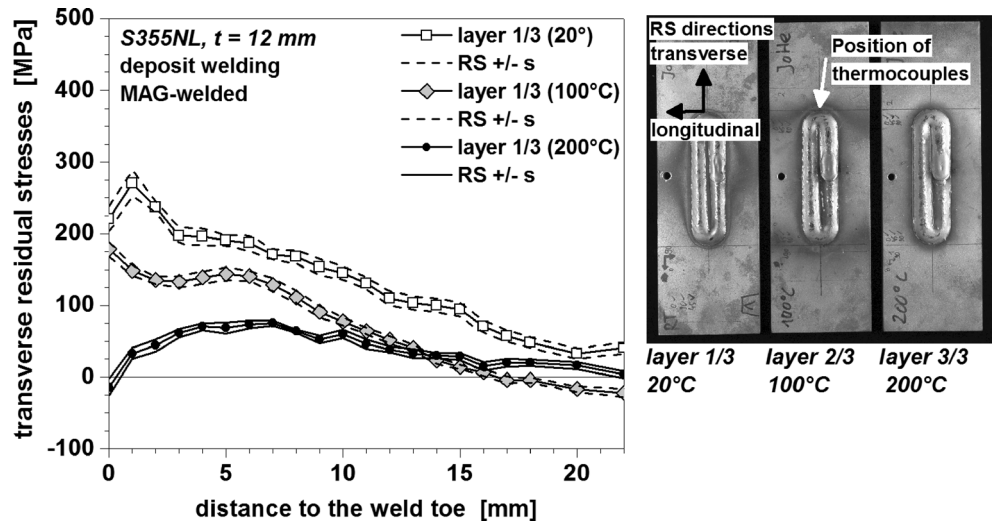
welding were similar to those from single-layer welds and from deposition welds and given in detail elsewhere [19]. The major difference between the multilayer weld and the single-layer weld were the preheating and the inter pass idle temperature used. S355NL samples were not preheated. S960QL samples were preheated to 150 °C which was also kept for the following layers. The weld sequence is given in Fig. 8. All corresponding layers (1–1, 2–2, and 3–3) from both sample sides were welded after each other. In addition this figure shows the tack-welded sample as well as the position of six K-type thermocouples (diameter 0.5 mm) used for the determination of $t_{8/5}$ cooling times. The temperature was measured on a base plate made of S355NL at the face sides of the stiffeners during welding of all three layers. The results of the temperature measurements for all three layers are shown in
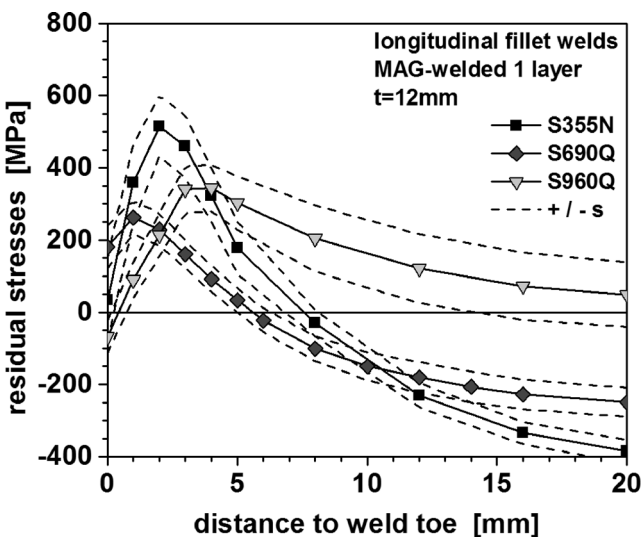
Fig. 7 Residual stresses in loading direction at the face sides of longitudinal single-layer fillet-welded stiffeners made from different steel grades [13]
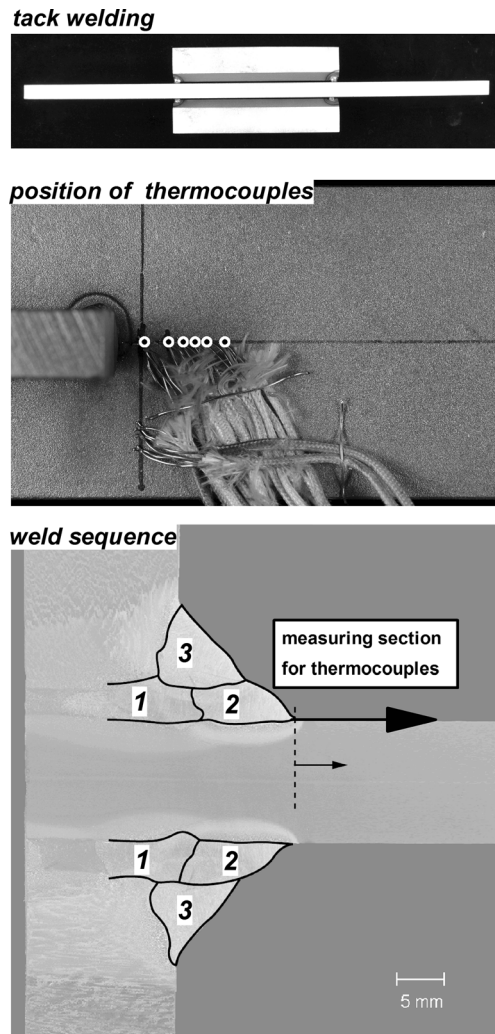
Fig. 8 Specimen before welding, locations of thermocouples and macrograph of multilayer weld with layer sequence

Fig. 9 Temperature over time during welding of each layer, measured on the base plate at the face sides of the stiffener
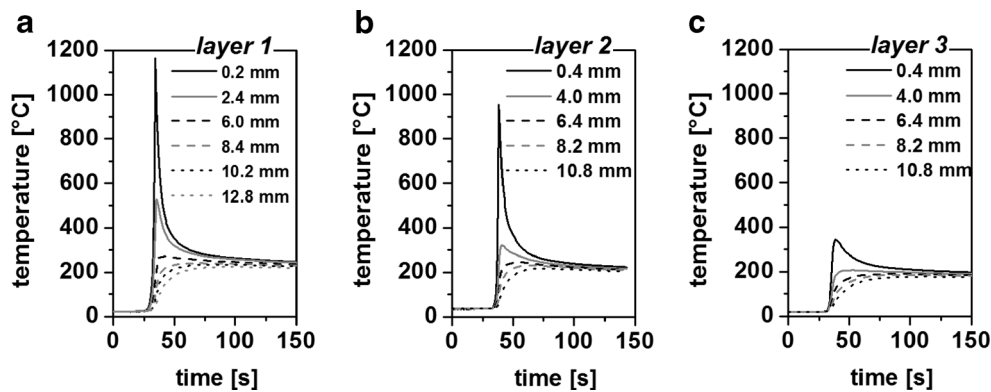

Fig. 9. In addition, this figure provides the distance to the fusion line of each thermocouple. The thermocouples were attached close to the fusion line during welding of the first and second layers. The third layer had no direct contact to the base plate since it was added on top of the first and second layers. One of the six thermocouples was burned during welding of the second layer. During welding of the root pass, the thermocouple 0.2 mm apart from the fusion line showed a peak temperature of 1,180 °C. The next thermocouple at a distance of 2.4 mm to the fusion line showed about 520 °C. The data from the first thermocouple allowed for the calculation of a $t_{8/5}$-time. It was determined to $t_{8/5}=6$ s. The highest temperature measured during welding of the second layer was about 970 °C. It was measured 0.4 mm apart the fusion line of the second weld layer. The cooling time from 800 to 500 °C was determined to 4.5 s. The welding of the third layer led to temperatures of 370 °C in the base metal 0.4 mm apart the fusion line of layer two.

Measurements by means of X-ray diffraction were also conducted on samples with multilayer fillet welds. The residual stress measurements were done in the same manner as described above for single-layer welds. Five samples of each material were measured at all four weld toes. Results are shown in Fig. 10 in terms of average values from all 20 measurements. In addition, the mean values of the standard deviations from the $\sin^2\Psi$-calculation are shown. The residual stress distribution from S355NL was comparable to the one shown for single-layer welds. The highest tensile residual stresses (320 MPa) were proven at a distance of approximately 2 mm from the weld toe. Residual stresses directly at the weld were considerably lower, with a mean value of 80 MPa. The residual stress profile from the investigated S960QL varied from the results of the single-layer welds. Residual stresses were very low at the weld toe (0 MPa) and decreased slightly with increasing distance to the weld toe (−100 MPa).

The longitudinal stiffeners with multilayer fillet-welded attachments were also investigated with regard to their residual stress through-thickness distribution. Neutron diffraction holds the potential for the determination of the residual stress profiles over specimen thickness. The results presented here are from measurements made with the E3 experiment at *Helmholtz Zentrum Berlin für Materialien und Energie* (BER II). Results from neutron diffraction are shown in Fig. 11: The position on the *x*-axis refers to the weld toe at the upper surface of the sample. It must be noted that the weld toe at the lower weld toe of the S355NL sample is shifted 1 to 1.5 mm to the left. The sample made of S355NL showed high tensile residual stresses at the surface, but the maximum was not located beneath the weld toe. It is shifted approximately 2 mm to the right into the base metal. The residual stresses dropped in thickness direction to nearly 0 MPa in the specimen center. Near the surface, the residual stresses also decreased with increasing distance to the weld toe. In case of the S960QL were two tension maxima found. They were located beneath the surface whereas residual stresses near the surface were considerably lower. That was also a result of the X-ray diffraction measurement where the residual stresses at the surface were found to be very low. The magnitude of the tensile maxima beneath the surface was in the range of 40 % of the yield strength of the base metal.
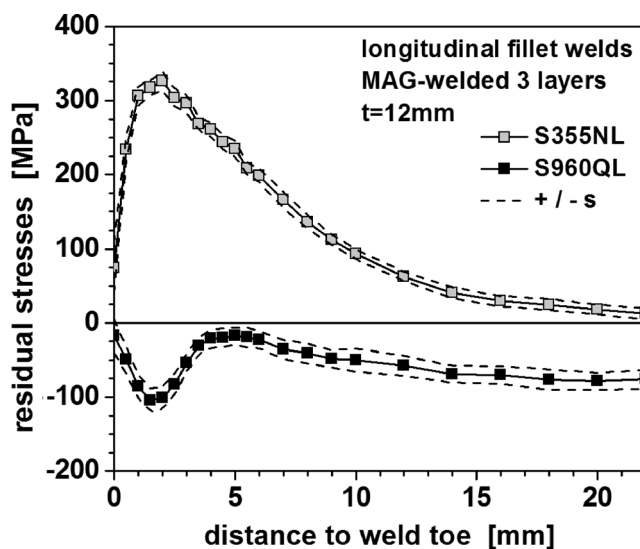
Fig. 10 Residual stresses in loading direction at the face sides of longitudinal multilayer fillet-welded stiffeners made from different steel grades

Fig. 11 Residual stresses in megapascal through thickness from a longitudinal stiffener made of S355NL (*left*) and S960QL (*right*)
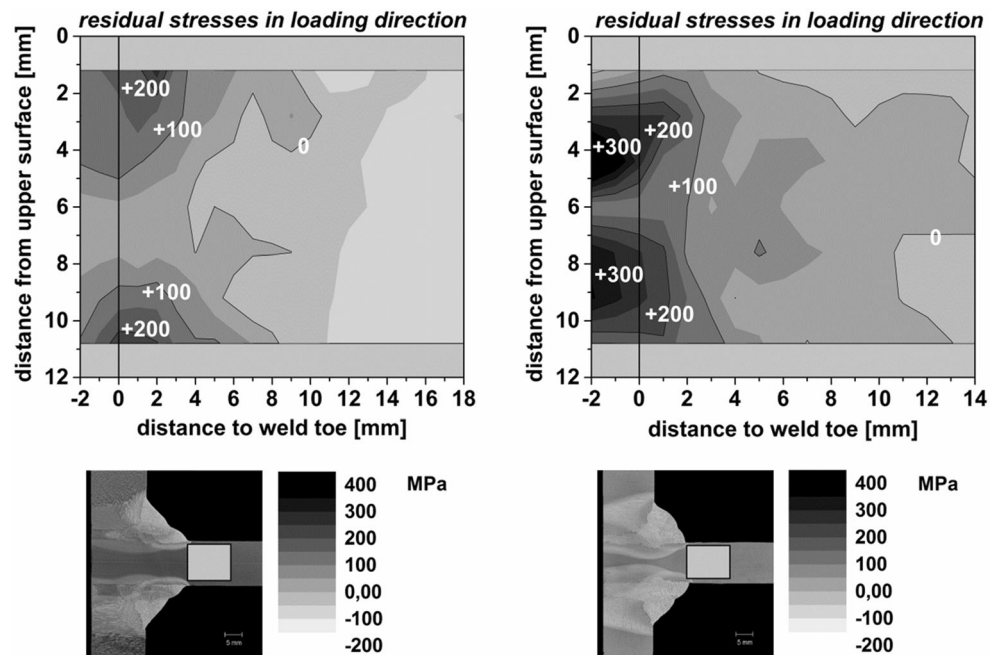
5 Finite element calculation

Welding residual stresses were also determined by means of a finite element calculation. The major benefit of residual stress calculations in comparison to welding experiments and residual stress measurements is the full access to all components of the results. For instance, the through-thickness distribution of residual stresses or principal stresses at all sample locations can be determined which is impossible to achieve by measurements. Calculations allow varying welding parameters easily and interpreting their effects. Nevertheless, the calculations must always be checked in terms of the calibration of the heat input by means of temperature measurements and the comparison to micrographs [20, 21].

Numerical investigations were used here to achieve better understanding of the influence of the austenite phase transformation in the HAZ on the final residual stress state. The material was varied to separate this effect from hindered shrinkage. For the purpose of this work, a longitudinal stiffener was modeled with a thickness of 10 mm and a single-layer fillet-weld. The width of the base plate was 80 mm and the length 350 mm. The gusset was attached only to one side of the base plate in the model to reduce calculation effort. The commercial program *Sysweld* (ESI-Group) was used for the residual stress calculations. The used material models were "S355 tempering" with isotropic hardening as a reference for transforming steels and an austenitic steel X5CrNi1810 (1.4301). Even though these steels are not comparable in strength (yield strength at 20 °C S355: f_y=360 MPa and X5CrNi1810: f_y=240 MPa) they allow a qualitative comparison of the effect of hindered volume expansion on the residual stresses after welding.

The element size in the close surroundings of the weld was set to 1 mm. The heat source was calibrated with experimentally determined time-temperature distributions at similar locations at the surface. Further, the molten zone was compared to the weld bead determined from micrographs (compare Fig. 12). To model the weld penetration and to ensure the full fusion of the filler material were two heat sources, a Goldak and a Gaussian heat source, coupled. If the HAZ, numerically and experimentally determined, are compared, one effect of the two heat sources can be seen, Fig. 12. The numerical model overestimates the size of the HAZ below the weld toe and the molten zone near the gusset as well as it underestimates the fusion below the weld. However, ensuring full fusion of the filler metal to the base metal at a high welding velocity, the use of two heat sources became necessary. The cooling time calculated 1 mm apart the weld toe was determined to 4.2 s which was comparable to results from welding experiments.

As an example of the results, the residual stresses in axial sample direction are presented in Fig. 13. Residual stresses transverse to the welding direction are shown after cooling to ambient temperature (*t*=800 s). Shown here are residual stress distributions from numerical investigations using both materials, S355 and X5CrNi1810. In comparison experimental results are shown from single-layer fillet-welded longitudinal stiffeners. In case of S355, the distribution of numerically and experimentally determined residual stresses was similar. However, the highest magnitudes as well as the location of the maxima differed. Experimentally determined residual stresses were considerably higher and the maximum was located closer to the weld toe. The derivation in the base metal was a consequence of the clean blasting process of the base

Fig. 12 *Left*: Comparison of numerically determined temperatures in the weld in degrees Celsius and a representative micrograph

| 1500 °C |
| 1352 °C |
| 1204 °C |
| 1056 °C |
| 908 °C |
| 760 °C |
| 612 °C |
| 464 °C |
| 316 °C |
| 168 °C |
| 20 °C |
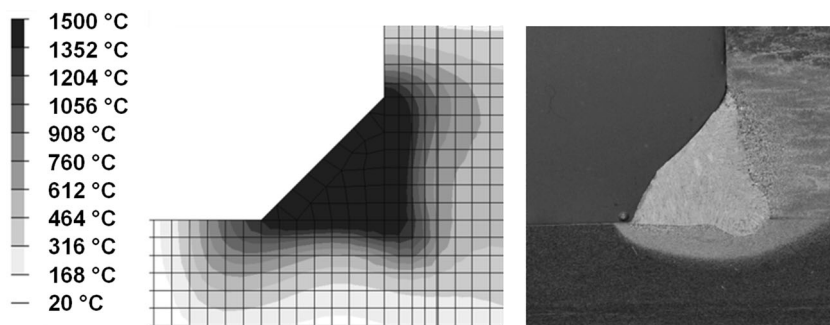
plates used as already mentioned earlier. Nevertheless, both residual stress distributions showed the drop of residual stresses close to the weld toe. This was not the case for the numerically modeled X5CrNi1810. The highest residual stresses were located directly at the weld toe.

Phase proportions in the adjacent area of the weld toe can be derived by looking further into the results from residual stress calculations, Fig. 14. Shown are the phase proportions along a line at the specimen surface and into plate thickness direction calculated from the S355-model.

The phase proportions were determined from the elements near the weld toe. At the surface (Fig. 14, left), one can see that in a distance up to 3 mm bainite and martensite phase were generated during cooling after welding. The same can be found over specimen depth (Fig. 14, right). The martensite proportion directly at the weld toe was about 40 %. The bainite proportion was even slightly higher. However, some retained austenite could be found (about 5 %). Over depth as well as at the surface one can see that the material volume, which did not transform into ferrite, is limited by a size of approximately 3 mm length and depth. That size correlates to the above shown results from residual stress distributions near the weld toe. Reduced residual stresses could be found in the

HAZ. This is an effect of the volume expansion at low transformation temperature.

6 Discussion

Residual stresses in longitudinal stiffeners have been studied in detail by experimental and numerical approaches for different steel grades. Additionally, a literature survey on residual stresses near the fatigue-relevant weld toe was conducted. On the whole, it can be seen that the results from literature are in good agreement with the presented own measurements. The heated weld tends to shrink after welding in longitudinal sample direction which is suppressed by the colder sides of the base plate. Consequently, high tensile residual stresses are generated below the fillet weld and the stiffener. But in most cases no high tensile residual stresses could be found in the HAZ. This effect can be explained by the influence of austenite phase transformation as described for longitudinal welds above. The results from the deposit welding experiments and the temperature measurements confirm this trend further.

The welding experiments with deposition welds (setup 1) show how residual stresses around such welds are affected by the cooling rate and the heat input. The residual stress generation is considerably affected by temperature balancing after welding. This was observed by welding multilayer deposition welds. The temperature balancing after welding of the first layer of the multilayer weld takes place almost homogeneously in the entire steel plate, see Fig. 5. The heat input spreads homogeneously in the steel plate. This means that, in terms of the effects shown in Figs. 3 and 4, the cooling rate is moderate and the phase transformation occurs consequently at relatively high temperatures. At the weld toe, the influence of hindered volume expansion during the phase transformation is relatively low. This effect can be further increased by preheating to 100 °C, see Fig. 6. This leads to an increase of the phase transformation temperature and a decreasing influence of the residual stresses from the hindered volume expansion. High tensile residual stresses are generated at the weld toe due to hindered shrinkage. A further increase of the preheating temperature to 200 °C leads to a clear decrease of the tensile residual stresses. The higher temperature of the entire
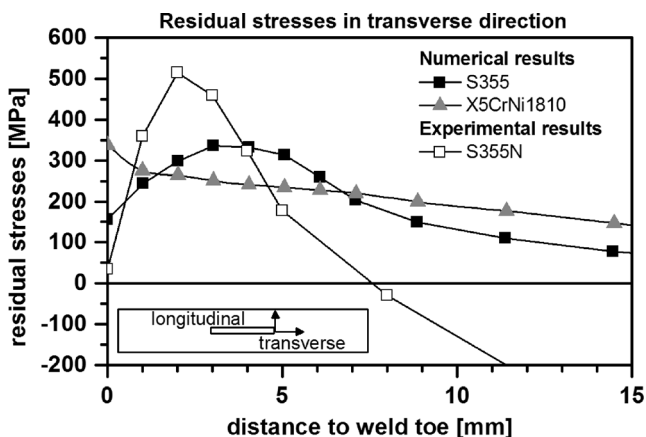
Fig. 13 *Left*: Determined residual stresses in megapascal in axial sample direction (in loading direction) from S355 (transforming steel). *Right*: Determined residual stresses in megapascal in axial sample direction (in loading direction) from austenitic 1.4301 (X5CrNi1810)
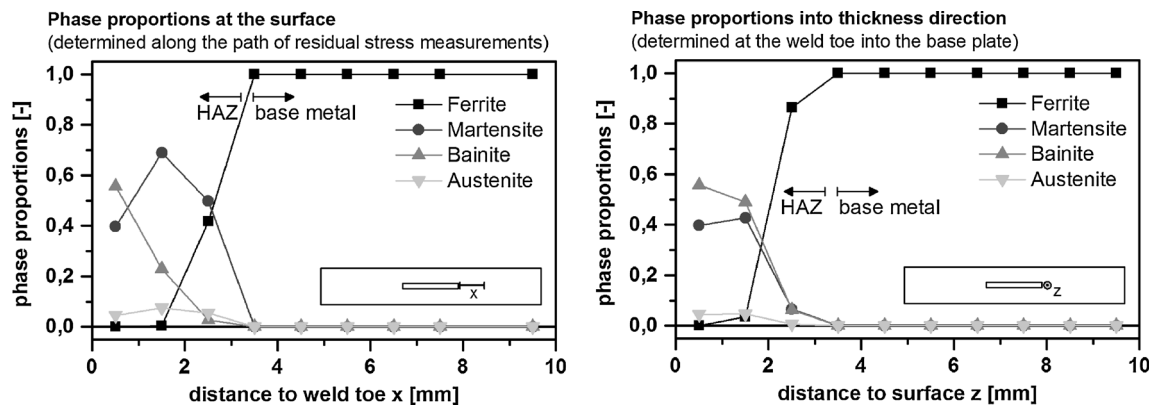
Fig. 14 Calculated phase proportions for S355. *Left*: Phase proportions over specimen thickness starting from the weld toe at the upper surface. *Right*: Phase proportions at the specimen surface starting from the weld toe into the base metal

specimen leads to a decrease of stiffness that again decreases the constraints during shrinkage. This effect was also explained in Fig. 4. The temperature balancing in the specimen during welding of the second layer of the multilayer weld (Fig. 5) is different from the first layer. The heat is concentrated in the middle of the specimen because of the accumulation of weld metal. This is also indicated by the tempering colors in the middle of the steel plate. In consequence this leads to a higher cooling rate at the short ends of the deposit weld. Correspondingly, the phase transformation occurs at lower temperatures, and compressive residual stresses from hindered volume expansion superpose the tensile residual stresses from hindered shrinkage. The welding of the third layer emphasizes this effect even more since material is accumulated in the middle of the steel plate and the heat is concentrated even stronger in the middle of the steel plate. The increasing tempering colors around the middle of the weld support this explanation and can also be seen in Fig. 6.

Observations regarding the influence of material properties can be made from experiment setup 2. Here different steel grades were used for welding small-scale samples with fillet welds. Residual stresses near the weld toe notable drop in the HAZ caused by austenite phase transformation. The highest residual stresses in all investigated construction steels were not located at the weld toe. At the weld toe low tensile residual stresses or even compressive residual stresses were observed. Higher yield strengths do not lead to higher residual stresses. In contrast, the highest residual stresses were observed in case of the mild steel S355NL. Interestingly the effect of austenite phase transformation was remarkable higher in case of S960Q compared to S355N or S690Q. For this material the tension maximum was determined further apart the weld toe.

Results from experimental setup 3 show final residual stresses at multilayer welds. In case of the mild steel S355NL similar residual stress profiles could be determined as for single-layer welds or deposition welds. The similarity can be explained by temperature–time measurements during welding of specimens with attached gussets. The temperature

profiles measured show clearly the rapid cooling at the face sides of the stiffeners. Short $t_{8/5}$-times of 5 s lead to phase transformation at relatively low temperatures (450 to 500 °C) and thus to martensite and bainite phases in the HAZ. Based on the model described above, this leads to hindered volume expansion during phase transformation combined with distinctive yield strength at elevated temperatures. Consequently low tensile or even compressive residual stresses can be expected in the HAZ. This residual stress generation model can be supported by the through-thickness distribution determined by neutron diffraction. Tension maxima were found here apart the weld toe as well. For samples made of S355N it was found by neutron diffraction that the surface residual stresses drop in thickness direction. In case of high-strength S960QL the highest tensile residual stresses were detected below the surface. This is remarkable and needs further investigations. A possible explanation is the applied preheating and inters pass idle temperature which decreases the stiffness during cooling. Results from both diffraction methods are in good agreement and are complementing each other.

Numerical investigations also support the described mechanism above. The phases in the HAZ determined by means of calibrated heat source and the used material model S355 are in agreement with observations from micrographs and time-temperature transformation diagrams, compare [22]. In case of S355, the residual stress distributions determined experimentally and numerically are comparable as well. Changing to non-transforming material X5CrNi1810 it can clearly be seen that the tension maximum is located at the weld toe. Hindered shrinkage after cooling is the only cause for residual stresses in this case. However, at this stage the results from numerical investigations do not precisely match the results from measurements in comparable real welds (S355). Derivations in terms of the magnitude of the residual stresses and the location of the residual stress maximum are proven. The maximum determined by means of the calculation is located approximately 5 mm from the weld toe, whereas X-ray measurements generally indicate the maximum to be 2 mm or 3 mm from the

weld toe. The calculated magnitude of the residual stress peak at the surface hardly matches the results from measurements. The tensile residual stress peak in depth direction overestimates the proven magnitudes from neutron diffraction by approximately 100 MPa. Both of these insufficiencies can most likely be explained by the used material model and the used heat source. The strength, the hardening and the phase transformation behavior of the used steel were not calibrated for the steel used for the experiments. Material properties have significant effect on the residual stress distribution as shown by experimental setup 2. Nevertheless, the calculations are of high value since they prove the general mechanism of residual stress distribution in such welds. The highest residual stresses from welding cannot be found at the weld toe due to effects from austenite phase transformation.

7 Conclusions

The presented residual stresses from deposition welds and also from single- and multilayer welded specimens are in good agreement with residual stress data from the presented literature. In addition, the discussed experiments pointed out that the results of residual stress generation in such welds are generally caused by a combination of hindered shrinkage during cooling and austenite phase transformation. The hindered shrinkage is a function of the geometry and the heat input. The welding conditions and the preheating temperature govern the cooling rates, especially at the short face sides of the stiffener. High energy input, e.g. in terms of preheating, leads to longer cooling times whereas under regular welding conditions very short $t_{8/5}$ times were observed for the investigated steels and specimen geometries. The phase transformation temperature depends on the cooling time and results in more or less distinctive yield strengths at elevated temperatures that constrain the occurring volume expansion. If the cooling speed is high, a high influence of that constrained volume expansion on the resulting residual stresses can be expected. The shrinkage constraint during cooling is depending on the temperature gradients in the specimen and is decreasing with increasing energy input.

It was found that the residual stresses at the weld toe are generally below the yield strength of the base metal. Further, in case of transforming construction steels it was found that the residual stresses at the weld toe are far below the maximum of the residual stresses. The maximum was observed some millimeters from the weld toe respectively below the specimen surface.

Summarizing, it can be said that the residual stress generation in steel plates with fillet-welded longitudinal gussets is generally affected by the described interacting effects of hindered shrinkage during cooling and hindered volume expansion during the phase transformation. High tensile residual stresses at the weld toe can be expected in cases where the cooling rate is relatively low and the geometric constraints are high. Both conditions are unlikely in case of welding small specimens used for fatigue testing in the laboratory scale. The theoretical mechanisms of residual stress generation described above can also be transferred to large scale structures. For practical applications the cooling time can be used as indicator for the influence of austenite phase transformation on final residual stresses. However, it is still to consider that thicker sheets or stiff structures may increase the shrinkage constraints and thus increase residual stresses.

References

1. Macherauch E, Wohlfahrt H (1985) Eigenspannungen und Ermüdung. In: Ermüdungsverhalten metallischer Werkstoffe, Deutsche Gesellschaft für Metallkunde e.V., Oberursel, pp. 237/83 (in German)
2. Radaj D Vormwaldt M (2007) Ermüdungsfestigkeit – Grundlagen für Ingenieure, 3. Ed. Springer (in German)
3. Nitschke-Pagel T (1994) Eigenspannungen und Schwingfestigkeit geschweißter Feinkornbaustähle. Dissertation TU Braunschweig (in German)
4. Sonsino CM (2007) Course of S-N-curves especially in the high-cycle fatigue regime with regard to component design and safety. Int J Fatigue 29:2246–2258
5. Hobbacher A (ed) (2009) Recommendations for fatigue design of welded joints and components. Welding Research Council, New York
6. Buxbaum O, Kulka C, Sonsino CM (1987) Verlauf der Wöhlerlinie von Schweißverbindungen bei hohen Schwingspielzahlen. LBF-Report Nr.4772, Fraunhofer-Institut für Betriebsfestigkeit, Darmstadt (in German)
7. Berge S, Eide O (1982) Residual stress and stress interaction in fatigue of welded joints. Residual Stress Effects in Fatigue, ASTM STP 776, American Society for Testing and Materials, pp. 115-131

8. Bogren J, Lopez Martinez L (1993) In: Blom AF (ed) Spectrum fatigue testing and residual stress measurements on non-load carrying fillet welded test specimens. Proceedings of the Nordic Conference on Fatigue. EMAS Publishers, West Midlands

9. Sakino Y, Sano Y, Kim Y (2007) Residual stress of steels for structure and fillet weld zone after laser peening. Trans JWRI 36(2):81–86

10. Varfolomeev I, Moroz S, Brand M, Siegele D, Baumgartner J (2011) Final report: Lebensdauerbewertung von Schweißverbindungen unter besonderer Berücksichtigung von Eigenspannungen. Bericht W 17/2011. Fraunhofer IWM, Fraunhofer LBF (in German)

11. Weich I (2009) Ermüdungsverhalten mechanisch nachbehandelter Schweißverbindungen in Abhängigkeit des Randschichtzustandes. Dissertation, TU Braunschweig (in German)

12. Stoschka M, Leitner M, Fössl T, Eichlseder W (2010) Application of fatigue approaches on fillet welds of high strength steel. Materialwiss Werkst 41(11):961–971

13. Nitschke-Pagel Th, Dilger K (2011) Residual stresses in welded steels with longitudinal stiffeners. Proceedings of the Twenty-first (2011) International Offshore and Polar Engineering Conference. Maui, Hawaii, USA, June 19-24, pp. 295-300

14. Hensel J, Nitschke-Pagel Th, Schönborn S, Dilger K (2012) Factors affecting the knee point position of S-N curves of welds with longitudinal stiffeners. IIW Document XIII-2441-12, International Institute of Welding, Paris

15. Kloos KH (1979) Residual Stresses, Definition and Causes of Generation. J Mat Technol 10:293–302

16. Nitschke-Pagel T, Dilger K (2006) Eigenspannungen in Schweißverbindungen - Teil 1: Ursachen der Eigenspannungsentstehung beim Schweißen. Schweißen und Schneiden 9:466–479, in German

17. Wohlfahrt (1986) Die Bedeutung der Austenitumwandlung für die Eigenspannungsentstehung beim Schweißen. Härterei-Technische-Mitteilungen 41 Nr.5, p. 248/257 (in German)

18. Nitschke-Pagel T, Wohlfahrt H (2002) In: Dias AM, Pina J, Batista AC, Diogo E (eds) Residual stresses in welded joints—sources and consequences. Proc. of the 6th European Conf. on Residual StressesTrans Tech Publications, Switzerland, pp 215–224

19. Schlussbericht Nk

20. Lindgren L-E (2006) Numerical modeling of welding. Comput Methods Appl Mech Eng 195(48):6710–6736, North-Holland

21. Yaghi A, Becker A (2004) State of the Art Review - Weld Simulation Using Finite Element Methods, Final report FENET-UNOTT-DLE-08, University of Nottingham

22. Seyffarth P, Meyer B, Scharff A (1992) Großer Atlas Schweiß-ZTU-Schaubilder. Schweißen und Schneiden, Düsseldorf (in German)